Tracking landslide displacements by multi-temporal DTMs: A combined aerial stereophotogrammetric and LIDAR approach in western Belgium

O. Dewitte [a,*], J.-C. Jasselette [b], Y. Cornet [c], M. Van Den Eeckhaut [d,e], A. Collignon [b], J. Poesen [d], A. Demoulin [a,f]

[a] Department of Geography, Unit of Physical Geography and Quaternary, University of Liège, Allée du 6 Août 2, 4000 Liège, Belgium
[b] Ministry of Equipment and Transport of the Walloon Region, Boulevard du Nord 8, B-5000 Namur, Belgium
[c] Department of Geography, Unit of Geomatics, University of Liège, Allée du 6 Août 17, B-4000 Liège, Belgium
[d] Physical and Regional Geography Research Group, K.U. Leuven, Celestijnenlaan 200-E, 3001 Heverlee, Belgium
[e] Post-doctoral fellowship, Fund for Scientific Research, Flanders, Belgium
[f] Belgian National Fund for Scientific Research, Belgium

ABSTRACT

The study of small and/or slow reactivations of landslides requires describing their displacements over decades, which may be done with accurate multi-temporal digital terrain models (DTMs). We applied aerial stereophotogrammetry to build the historical topographies of old deep-seated landslides close to Oudenaarde in the Flemish Ardennes (West Belgium) at different dates. Three precise aerotriangulations (1996, 1973, 1952) were carried out. After capturing the ground data manually from the stereomodels, 2 m-resolution DTMs were interpolated by kriging, with a final accuracy ranging between ~45 cm and ~65 cm. Another DTM was interpolated with an accuracy of ~30 cm from airborne LIDAR data acquired in 2002. Differential DTMs were produced to identify vertical and horizontal ground displacements over the 1952–2002 period. We describe here the kinematics of a particularly active landslide with a well-documented recent activity. Until the first half of the 90 s, little activity of the landslide was detected. In February 1995 a reactivation event caused vertical displacements of up to −7 m along the main scarp and up to +4 m in the accumulation zone. Horizontal movements of 4 to 10 m are also inferred. These topographic changes correspond to reactivated slip along the rotational basal shear surface. In the same time, the main scarp retreated by up to 20 m. The reactivation, favoured by several anthropogenic factors (e.g. loading, impeded drainage), was triggered by intense rainfall. Between 1996 and 2002, the observed displacements correspond to limited scarp retreat (≤4 m) and compaction of the slipped mass, partly enhanced by artificial drainage.

© 2008 Elsevier B.V. All rights reserved.

1. Introduction

The understanding of landslide mechanisms is greatly facilitated when information on their horizontal and vertical displacements is available. Geodetic techniques, recently in particular GPS, are commonly used to monitor ground motion with a high accuracy (Malet et al., 2002; Coe et al., 2003; Squarzoni et al., 2005; Brückl et al., 2006; Demoulin, 2006). However, they require access to the site and may be time-consuming if the information has to be densified, spatially and/or temporally. Moreover such studies generally encompass a time interval of a few years at maximum, thus providing poor information on longer-term landslide kinematics.

According to the scale, accuracy and resolution needed, several techniques of remote sensing are available to build digital terrain models (DTMs) of landslides (Mantovani et al., 1996; Metternicht et al., 2005). In the case of the Flemish Ardennes (Fig. 1), the ground displacements are rather small (in the order of few meters) and slow, and their reliable description requires a final DTM accuracy better than 1 m in the three directions. Several techniques such as GB_InSAR (Tarchi et al., 2003; Antonello et al., 2004), LIDAR (McKean and Roering, 2004; Chen et al., 2006; Glenn et al., 2006), GPS (Higgitt and Warburton, 1999; Nico et al., 2005; Demoulin, 2006), and aerial photogrammetry (Chandler, 1999; Hancock and Willgoose, 2001) are capable of supplying such accurate 3D topographic data. However, only the stereophotogrammetric analysis of aerial photographs can cover several decades of observation (Hapke, 2005).

The main objective of this research is to assess how reliable landslide small displacements can be measured from multi-temporal DTMs produced by aerial stereophotogrammetry. For this purpose, we used classical aerial photographs at scales ranging between 1:18500 and 25000 (Table 1), which required careful measurements at each step of the DTM production in order to reach a submeter accuracy (Kraus and Waldhäusl, 1994; Kasser and Egels, 2001). A detailed analysis of the precision, accuracy and reliability associated with each step of the DTM extraction procedure is therefore given. We present first the

* Corresponding author. Tel.: +32 43 665255; fax: +32 43 665722.
  E-mail address: odewitte@ulg.ac.be (O. Dewitte).
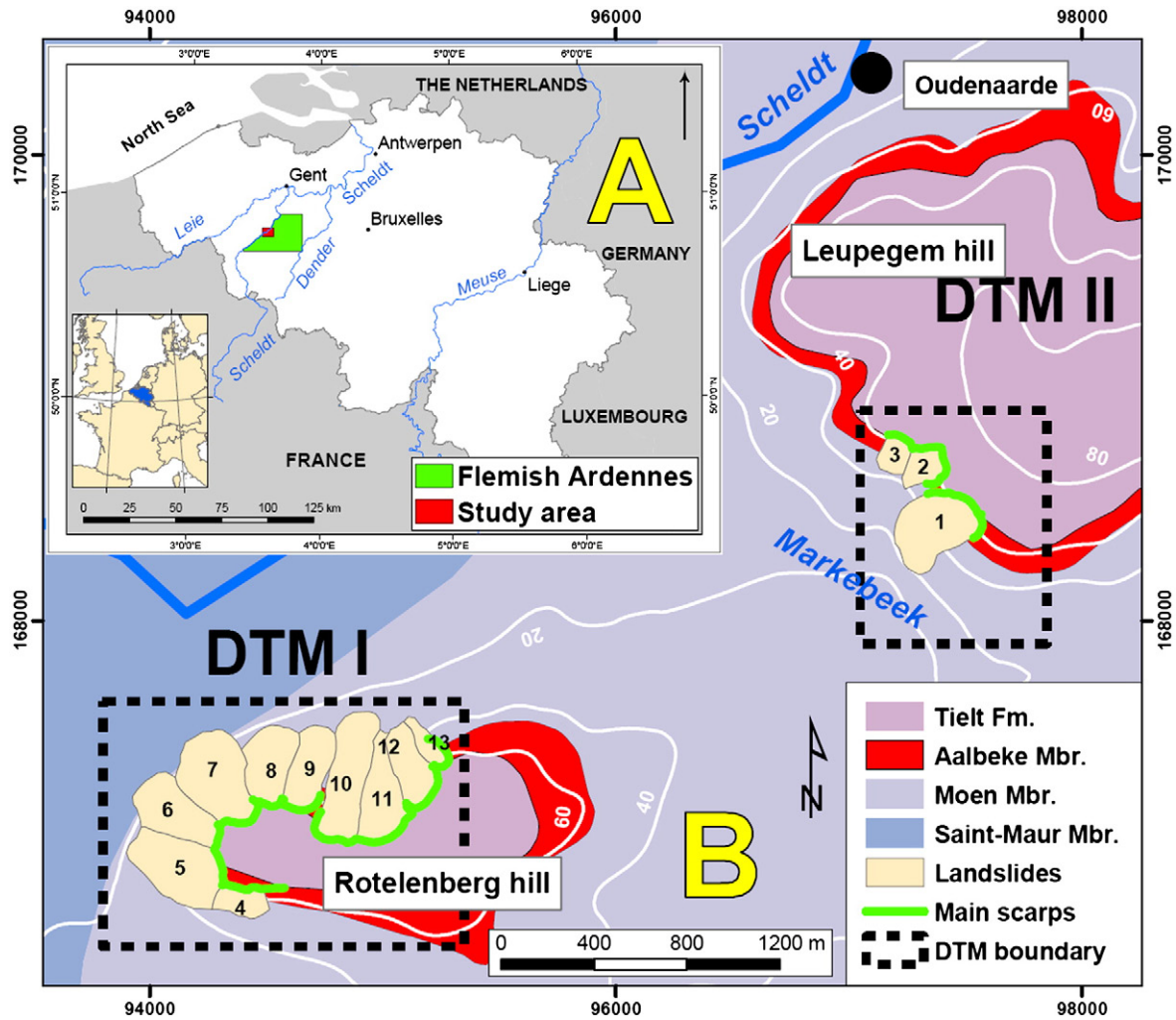
Fig. 1. (A) Location map of the Flemish Ardennes and the study area. (B) Location of the two studied hills with the lithological setting, and the boundaries and main scarps of the 13 landslides considered in the analysis. The quadrangles DTM I and DTM II delimit the two areas where the DTMs were extracted.

photogrammetric procedure applied to the photographs. Details on the subsequent DTM construction and on a LIDAR-derived DTM provided by the Flemish Government (DEM of Flanders, 2007) are also given. We then show how vertical and horizontal landslide motions can be inferred from DTM subtraction, focusing on one particular landslide, whose activity is well documented over the last 50 years.

2. Study area

In West Belgium, Van Den Eeckhaut et al. (2005) mapped more than 150 large deep-seated landslides within the loose Tertiary sediments of the hilly area of the Flemish Ardennes (Fig. 1). All landslides predate 1900 AD and might have been initiated under periglacial conditions, possibly in response to a seismic trigger associated with a period of heavy rainfall (Van Den Eeckhaut, 2006; Van Den Eeckhaut et al., 2007b). According to the Keefer's relation between maximum distance of landslides from fault and Richter magnitude M_L (Keefer, 1984), Van Den Eeckhaut (2006) estimated magnitudes between 5 and 6 to trigger landslides in the Flemish Ardennes. However, the biggest earthquake recorded in Belgium during the 20th century occurred within the Flemish Ardennes in June 1938 and, despite a magnitude M_L of 5.6, no landslide was reported.

This research focuses on two hills affected by 13 landslides close to the town of Oudenaarde and situated along the river Scheldt at altitudes between 75 and 80 m a.s.l. (Fig. 1). The landslides are carved

in an alternation of Eocene subhorizontal clayey sand and clay layers on which a perched water table can expand (Jacobs et al., 1999). The 13 landslides are in contact with the Aalbeke Member of the Kortrijk Formation, which consists of 10-m-thick homogeneous blue massive clays and has been recognized as the layer most sensitive to landsliding (Fig. 1). The mean landslide size is ~6 ha and their main

Table 1
Main characteristics of the photograph negatives used for the digital stereophotogrammetry

Aerial photographs	1996[a]	1973	1952
Date	15-04	27-04	17-04
Image size	23×23 cm	23×23 cm	18×18 cm
Overlap	~60%	~60%	~60%
Flight height	~3130 m	~2830 m	~3750 m
Camera	WILD LEITZ LTD	WILD LEITZ LTD	N
Camera type	RC10	N	N
Lens type	15 UAG II 3020	Uag 282	N
Focal length	153.05 mm[b]	153.16 mm[b]	150 mm
Fiducial marks	Yes	Yes	N
Scale	~1:20 500	~1:18 500	~1:25 000
IGN photograph number	1437, 1438, 1439	1418, 1419, 1420, 1421	177, 178, 179, 180

N: no information; Yes: information available.
[a] With the camera calibration certificate (date: February 1989).
[b] Calibrated focal length.

scarp, with a height of ~8 m, makes the abrupt fringe of the plateaus (Dewitte and Demoulin, 2005; Dewitte et al., 2006). They developed on slopes of 13–20%, preferentially oriented to the W and N. The mean value of the depth of the surface of rupture has been estimated in the range 30–70 m, implying displaced volumes between 670 000 m³ and 1 500 000 m³.

3. Photogrammetric operations

Aerial photographs are frequently used in digital photogrammetry to extract landslide relief (e.g. Oka, 1998; Weber and Herrmann, 2000; Kääb, 2002; Baldi et al., 2005; Casson et al., 2005; Hapke, 2005; Lantuit and Pollard, 2005). We selected only the aerial covers supplied by the National Geographical Institute (NGI) of Belgium that were taken at the beginning of the spring (when the trees are leaveless) in order to obtain a better restitution of the landslide areas under forest. We thus used the photograph negatives of the 1952, 1973 and 1996 covers, allowing the investigation of the landslide kinematics over a 44-year period (Table 1).

The image processing (Fig. 2) was performed using the Leica Helava Digital Photogrammetric Workstation DPW 300 with the software SOCET SET v4.3.1b (LH Systems, 1999). The photograph negatives were scanned with the LH Systems DSW 300 Digital Scanning Workstation with a pixel resolution of 12.5 μm that corresponds to a ground resolution of approximately 20 to 30 cm (Table 2).

3.1. Interior orientation

The interior orientation was carried out during the scanning operation (Fig. 2) by using the parameters of the camera established by the geometric calibration (Table 1). The radial distortion was only considered for the 1996 negatives for which a camera calibration certificate was provided. For the covers of 1973 and 1952, the radial distortion was not implemented and dummy fiducial marks were used for the 1952 negatives.

Fig. 2. Flow chart of the photogrammetric operations carried out to capture the 3D morphology of the landslides.

Table 2
Root mean square error (RMSE) of the interior orientation

Year	1996	1973	1952
Pixel size (μm)	12.5	12.5	12.5
Ground sample distance (cm)	25.6	23.1	31.3
Image RMSE (μm)	2.0	2.1	4.6
Ground RMSE (cm)	4.1	4.4	9.5

The final accuracies of the interior orientation are shown in Table 2. With accuracy values better than 10 cm, we may consider that the root mean square error (RMSE) of this orientation will not act significantly upon the final accuracy of the stereomodels. The larger error of 1952 is probably due to the use of less reliable fiducial marks.

3.2. Aerotriangulation

The aerotriangulation of the digital photos was performed by using an iterative least-square bundle block adjustment allowing simultaneously the relative and the absolute orientations of the photographs in the block (Kraus and Waldhäusl, 1994; Mikhail et al., 2001). The absolute orientation of the block requires the use of ground control points and the block adjustment accuracy is evaluated using check points with known ground coordinates (Fig. 2) which are not used as control in the solution. Moreover, control points and check points must be accurate enough to reflect the actual state of the ground surface.

A total of 26 photo-identifiable ground control points and check points acquired by GPS in February 2002 were used for the adjustments. The measurements were carried out by differential GPS in rapid static mode involving baselines of 1 to 6 km length. The uncertainty on the baseline components (N, E, and Up) is ~2–3 cm. Absolute positioning of the control and check points relies on the inclusion of five NGI points of known coordinates within the GPS network. The final uncertainty on the coordinates of the control and check points does not exceed 10 cm (Dewitte, 2006), thus remaining far below that of the block adjustment. Note that the GPS points were measured at places very easy to locate on the 1996 photographs (electric poles, fences, crossroads, etc.).

Three aerotriangulations were built, one for each covering date (Table 3). Each bundle block adjustment requires overabundant data to attribute X, Y and Z ground coordinates to each tie point (Kraus and Waldhäusl, 1994; Mikhail et al., 2001). As stressed by LH Systems (1999), the number of required points to obtain a logic solution depends on the number of image parameters adjusted, the number of images each point appears on, and the availability of the ground points (Table 3). For each image to adjust, 6 orientation parameters need to be computed. Each tie point contributes 3 unknowns (ground X, Y, Z) but provides 2 knowns (line ξ and sample η) for each image it is measured on. A ground control point brings more knowns than a tie point since some or all its ground coordinates are known.

The first stereomodel was adjusted with the three photographs of 1996 and 16 ground control points (Table 3). Each of these points was measured on two images (4 knowns) and its 3 ground coordinates (XYZ) were provided too (3 knowns). The adjustment of the 1996 stereomodel was performed in ideal conditions since all the parameters of the interior orientation were provided and the image quality was very high. The tie points were automatically measured before being interactively reviewed and corrected whereas the image positioning of the control points acquired by GPS (Fig. 2) was made manually in stereoscopy. Moreover, the control points were easy to locate.

However, the positioning of control points on historical photographs is far more difficult (Hapke, 2005). To avoid inaccuracies associated with the positioning of these points, the two stereomodels of
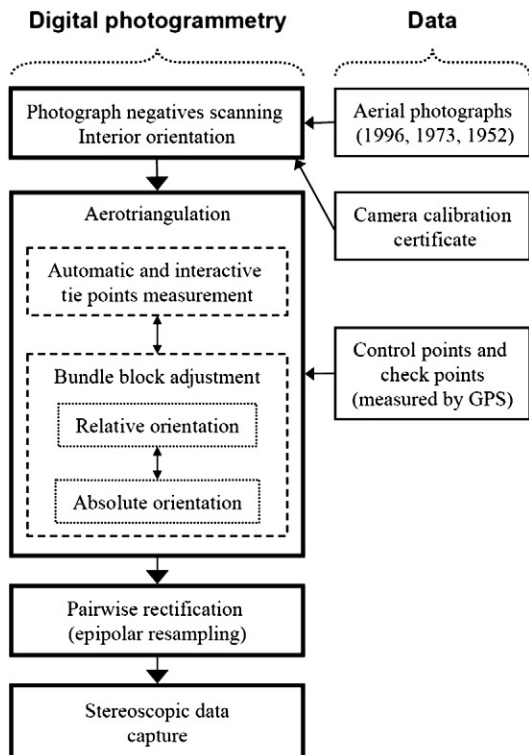
Table 3
Main characteristics of the 3 aerotriangulations of 1996, 1973 and 1952

Year	Orientation				Ground points		Control points			Tie points (TP)				Redundancy (R)	
	No. of images	No. of stereo pairs	No. of iterations	Orientation parameters[a]	#	XYZ	#	XYZ	ξη	#	P/TP	# P/TP	ξη	R[b]	%R[c]
1996	3	2	3	18	75	225	16	48	64	59	2 (4) 3 (6)	51 8	204 48	+121	161%
1973	4	3	3	24	61	183	0	0	0	61	2 (4) 3 (6) 4 (8) 5 (10) 6 (12)	22 12 19 7 1	88 72 152 70 12	+187	307%
1952	4	3	3	24	94	282	0	0	0	94	2 (4) 3(6) 4 (8) 5 (10) 6 (12)	32 35 19 7 1	128 210 152 70 12	+266	283%

The unknowns are the orientation parameters of the images and the adjusted XYZ coordinates of the homologous points. The knowns are the XYZ coordinates of the ground control points and the ξ and η image coordinates of the control points and tie points.

\#: number of measured points; XYZ: ground coordinates; ξη: image coordinates; P/TP: number of aerial photographs (or homologous rays) by tie point (the number of data by point is indicated between brackets); # P/TP: type of tie point.

[a] Underlined means unknown and double underlined means known.
[b] Redundancy (R) = knowns − unknowns.
[c] R / # ground points.

1973 and 1952 were rectified relative to the 1996 stereomodel (Hapke, 2005). For each new aerotriangulation, the images were placed in a second strip associated with the 1996 model whose adjusted orientation parameters had been blocked. The two other stereomodels were thus constructed by including the orientation parameters of 1996. Therefore, only tie points whose absolute XYZ coordinates are computed in the model of 1996 were necessary for the construction of the 1973 and 1952 aerotriangulations (Table 3). The tie points common to 1996 and either 1973 or 1952 acted here as control for the absolute orientation. All the points used in the three aerotriangulations were chosen outside the landslides in order to rely on stable places only (Berthier et al., 2005).

The measurement redundancy (LH Systems, 1999; Mikhail et al., 2001) is positive for the three bundle block adjustments (Table 3) and the required condition of overabundant data is therefore fulfilled. Moreover, the percent redundancy, defined as the ratio between redundancy and total number of ground points, is higher than the 50% value recommended by LH Systems (1999), giving to the solution a more consistent and meaningful residual RMSE value.

3.3. Evaluation of the aerotriangulations

A qualitative and a statistical evaluation of the aerotriangulations were carried out to ascertain that the block adjustments meet our requirements and are valid.

The qualitative evaluation consisted in displaying the residuals of the aerotriangulations (Figs. 3 and 4) in order to understand broad trends and to catch bad inputs. The ground points are distributed uniformly in the three stereomodels and the image residuals are smallest in the 1996 model (Fig. 3). The image residuals of the 1973 and 1952 adjustments point in random directions and have comparable sizes around the model centres where the landslides are located (Fig. 3). On the contrary, the size of the 1996 residuals often varies considerably from one point to another. This might result from too tight constraints applied to the ground control points, which did not allow them to adjust enough (Dewitte, 2006). As the residuals were very close to the maximum precision of 0.5 pixel announced by LH Systems (1999) (Table 4), the small E–W trend observed in the 1996 model was neglected.

The check points we used were placed close to the two investigated landslide areas (Fig. 4). No deformation appears in the block of 1996 and 1973, whereas the SW part of the 1952 model is slightly higher. The errors are randomly distributed and of comparable sizes.

In brief, the qualitative evaluation shows that the three aerotriangulations are reliable and respond to the requirements of this study. Like the image residuals (Fig. 3), the XYZ residuals (Fig. 4) of 1996 are the lowest and those of 1952 the biggest.

The statistical evaluation of the adjustments was performed by computing the precision and the accuracy of the measurements. The fact that the mean of the image residuals is very close to zero in the three models (Table 4) suggests that we are in the "ideal case" where the residuals may be treated as normally distributed random variables (Buiten and van Putten, 1997; Mikhail et al., 2001). The precision of the solution is given by the standard deviation of the image residuals of the ground points. For the 1996 aerotriangulation, the total standard deviation lower than 1 pixel satisfies the quality criterion given by LH Systems (1999) (Table 4). The somewhat lower precision of the two other solutions is not due to bad measurements of ground points. Rather, the measurement of the tie points of 1973 and 1952 using their coordinates in the 1996 images implied a combination of the errors of both models. Moreover, the resolution of the 1952 images is coarser (Table 2).

We estimated the accuracy of the solutions with 8 to 10 check points measured by GPS (Table 4). The evaluation was based on the RMSE of the check point differences between the computed co-ordinates generated for each block and the ground truth (GPS values). Since it was more than one order of magnitude better than the accuracy required for the final DTMs, the accuracy of the GPS measurements was not considered in the RMSE computations. Although the number of check points is not very high, they are located close to the landslide areas and we thus consider that they yield reliable results. If the errors are assumed to be normally distributed and independent, they can be used as standard deviation and the combined variance of independent variables is given by the sum of the individual variables variances (Borradaile, 2003). The horizontal RMSE values are similar to the vertical RMSE values and the worst values are observed in the 1952 aerotriangulation (Table 4). The global RMSE values range between ~22 cm and ~55 cm for the three stereomodels and are in agreement with the theoretical values proposed by Kraus and Waldhäusl (1994) and by Kasser and Egels (2001).

With respect to our goal, which is to locate vertical ground movements >1 m, the qualitative and statistical evaluations have shown

1996 (2000 ×)

1973 (500 ×)

1952 (500 ×)

Legend

○ Tie point

● Ground control point

— Image residual

⌀ Landslide

▭ Area of stereo extraction
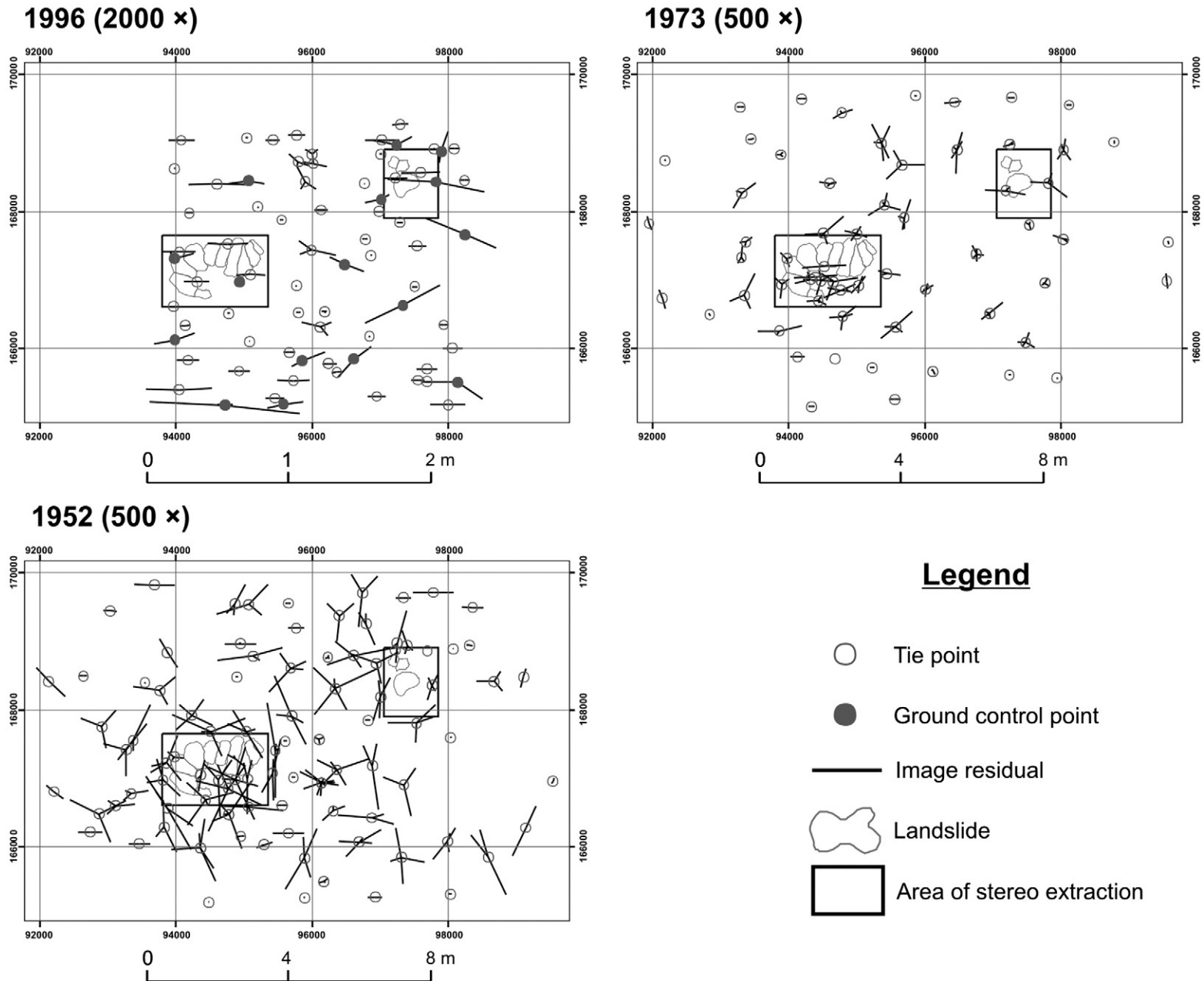
Fig. 3. Image residuals of the ground points used in the three aerotriangulations (1996, 1973 and 1952). The ground points (tie points and ground control points) are placed at their initial location. The residuals indicate thus the direction and the range of their displacements towards their adjusted locations. For example, a point whose residual is oriented towards the east is a point which has undergone during its adjustment a displacement towards the east. A ground point with two residuals is a point measured in two images. The image residuals are exaggerated 2000× in the block of 1996 and 500× in the blocks of 1973 and 1952.
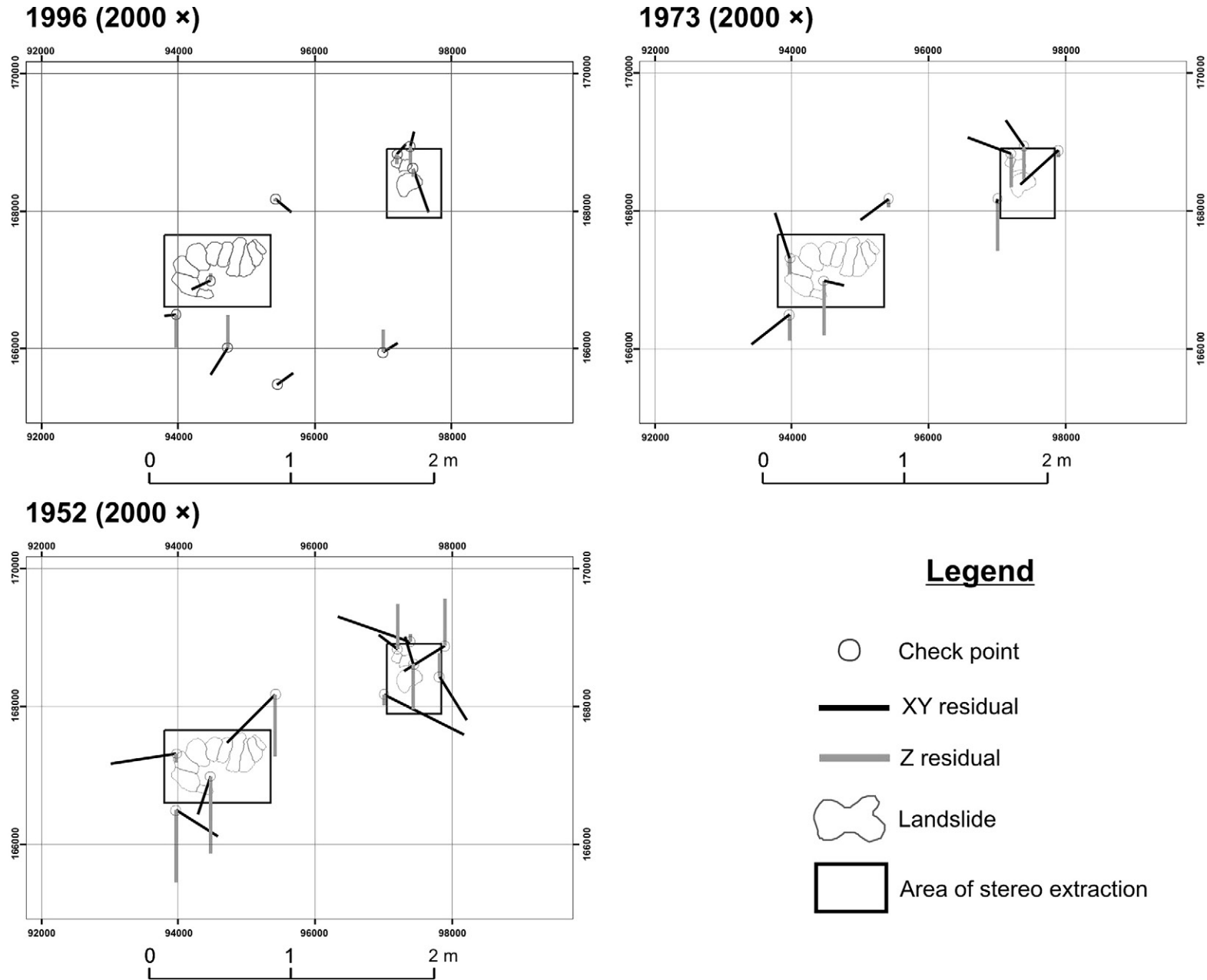
Fig. 4. *XYZ* residuals of the check points used in the three aerotriangulations (1996, 1973 and 1952).The check points are placed at their adjusted location. The residuals indicate the location error of these points compared to the ground coordinates measured by GPS. For example, a negative residual in *Z* (a *Z* residual is positive towards the north and negative towards the south) means that the adjusted point of the model is at an altitude higher than the GPS-defined altitude of the point; a positive residual in *XY* (a residual in *XY* is positive towards the east and negative towards the west) indicates that the adjusted point of the model is at the west of the point measured by GPS. The *XYZ* residuals are exaggerated 2000× in the 3 blocks.

Table 4
Precision and accuracy of the 1996, 1973 and 1952 aerotriangulations

			Year		
			1996	1973	1952
Precision	Mean of the image residuals	Pixel	1×10^{-4} (1×10^{-3})[a]	-7×10^{-4}	1×10^{-4}
	Total standard deviation	Pixel	0.49	1.42	1.99
		m	0.13	0.33	0.62
			No. of check points		
			9	8	10
Accuracy	RMSE (m)	σX	0.106	0.209	0.350
		σY	0.142	0.191	0.231
		σXY[b]	0.177	0.283	0.419
		σZ	0.147	0.244	0.343
		σTotal[c]	0.225	0.373	0.542

[a] Mean of the image residuals of the ground control points.
[b] $\sigma XY = \sqrt{\sigma X^2 + \sigma Y^2}$.
[c] σTotal $= \sqrt{\sigma X^2 + \sigma Y^2 + \sigma Z^2}$.

that the three stereomodels are of sufficient reliability, precision, and accuracy.

3.4. Stereoscopic data capture

The automatic terrain extraction methods provided with SOCET SET were not able to generate the DTMs accurately in many places, especially in the forested areas (Chandler, 1999; Fabris and Pesci, 2005). The stereoscopic data capture of spot heights (ground points) and breaklines (scarps, roads, water bodies) on the landscape surface was therefore carried out visually. The spot heights were extracted approximately every 10 m, but with a higher density in more contrasted topography, in particular within the landslides. In total, six areas were surveyed, i.e. the two investigated hills at three different dates (Fig. 1).

4. DTM construction

The captured elevation data were interpolated by ordinary kriging with the SURFER 8.0 software. Ordinary kriging is one of the most widely-used method in geostatistics and it has proved very effective in the interpolation of topographic data for the generation of DTMs (e.g. Siska et al., 2005; Chaplot et al., 2006). Through the use of semi-variograms, the kriging method considers the spatial autocorrelation in the topographic data (Goovaerts, 1997). This interpolation method also allows the insertion of breaklines which depict abrupt changes in elevation and increase the accuracy of the DTMs.

All six DTMs were interpolated by using an omnidirectional semivariogram adjusted with a power model (Goovaerts, 1997). Taking into account the data density, their spatial autocorrelation shown by the semivariograms, the precision and the accuracy of the stereomodels, the DTM grids were generated at a 2-m resolution. The vertical RMSE of the kriging interpolations obtained by cross-validation is ~40 cm (Table 5). The slightly higher error value of the 1996 DTM of the Leupegem hill with respect to that of the Rotelenberg is the consequence of its higher topographic variability due to the recent reactivation of landslide 1 (Fig. 1).

Assuming that the kriging and aerotriangulation errors are normally distributed and independent, the total vertical errors of the DTMs range from 0.4 to 0.5 m (Table 5) and the total 3D errors range between ~0.45 and ~0.65 m, which corresponds to values far below our required 1 m accuracy for the final DTM.

At the end of 2002, airborne LIDAR (Light Detection and Ranging) data were acquired over the study area by the Flemish Government with a point density of 1 point per 4 m^2. After correcting the dataset

Table 5
Accuracy of the DTMs

	Leupegem hill				Rotenlenberg hill			
Year	1996	1973	1952	2002[b]	1996	1973	1952	2002[b]
	m				m			
Kriging RMSE (Z)	0.461	0.390	0.391		0.389	0.372	0.385	
Aero. RMSE (Z)[a]	0.147	0.244	0.343		0.147	0.244	0.343	
Total RMSE (Z)	0.484	0.460	0.520	0.30	0.416	0.444	0.516	0.30
XY RMSE[a]	0.177	0.283	0.419		0.177	0.283	0.419	
Total RMSE (XYZ)	0.515	0.540	0.668		0.452	0.527	0.665	

[a] These values for the aerotriangulation are taken from Table 4.
[b] LIDAR-derived DTM.

for canopy and building returns (DEM of Flanders, 2007), a database with a point density of at least 1 per 20 m^2 was provided with an accuracy varying according to the land cover type (vertical RMSE of at worst 0.20 m under forest or better). Using a TIN interpolation, we then derived from the LIDAR data a DTM with a resolution of 2 m. The maximum vertical error of the interpolation being 0.2 m (Dewitte, 2006), the total RMSE in Z for the 2002 DTM equals ~0.30 m (Table 5).

5. Results: 1952–2002 evolution of a typical landslide

As an example, we detail the movements recorded for the landslide 1 of the Leupegem hill (Fig. 1). According to size and lithology, this landslide is representative not only of those of the Leupegem and Rotelenberg hills but also of those of the whole Flemish Ardennes (Dewitte and Demoulin, 2005). Moreover, its reactivation in February 1995 caused comparatively large ground displacements, and eyewitness reports of its evolution over the past 50 years are available (Van Den Eeckhaut et al., 2007a), allowing some qualitative validation of the measured displacements. This landslide extends over an area of ~9 ha and has a total length of 370 m and a maximum width of 260 m. The maximum height of its main scarp is 9 m. Through morphometric measurements, Dewitte and Demoulin (2005) estimated the depth of the rupture surface and volume before movement. Supposing a single rotational earth slide, they have computed a pre-landslide volume of 1 250 000 m^3 for a depth of the surface of rupture of 40 m.

5.1. Vertical displacements

A simple DTM subtraction yields a direct estimate of the vertical displacement of each landslide pixel during the considered time interval (e.g. Oka, 1998; Weber and Herrmann, 2000; Gentili et al., 2002; Kääb, 2002; van Westen and Getahun, 2003; Baldi et al., 2005; Casson et al., 2005; Hapke, 2005; Lantuit and Pollard, 2005; Brückl et al., 2006; Chen et al., 2006; Demoulin 2006). DTM subtraction implies that individual DTM errors can be combined as independent

Table 6
Accuracy and confidence intervals of the DTM subtractions

	Leupegem				Rotelenberg			
	68.3%[a]		95%[b]		68.3%		95%	
	XY (m)	Z (m)	XY (m)	Z (m)	XY (m)	Z (m)	XY (m)	Z (m)
DTM subtraction	$\pm 1.55\sigma$	$\pm 1.00\sigma$	$\pm 2.45\sigma$	$\pm 1.96\sigma$	$\pm 1.55\sigma$	$\pm 1.00\sigma$	$\pm 2.45\sigma$	$\pm 1.96\sigma$
2002–1996		±0.57		±1.12		±0.52		±1.00
1996–1952	±0.71	±0.71	±1.11	±1.39	±0.71	±0.66	±1.11	±1.30
1996–1973	±0.52	±0.67	±0.82	±1.31	±0.52	±0.61	±0.82	±1.19
1973–1952	±0.78	±0.69	±1.24	±1.36	±0.78	±0.68	±1.24	±1.33

[a] 68.3% confidence interval.
[b] 95% confidence interval.
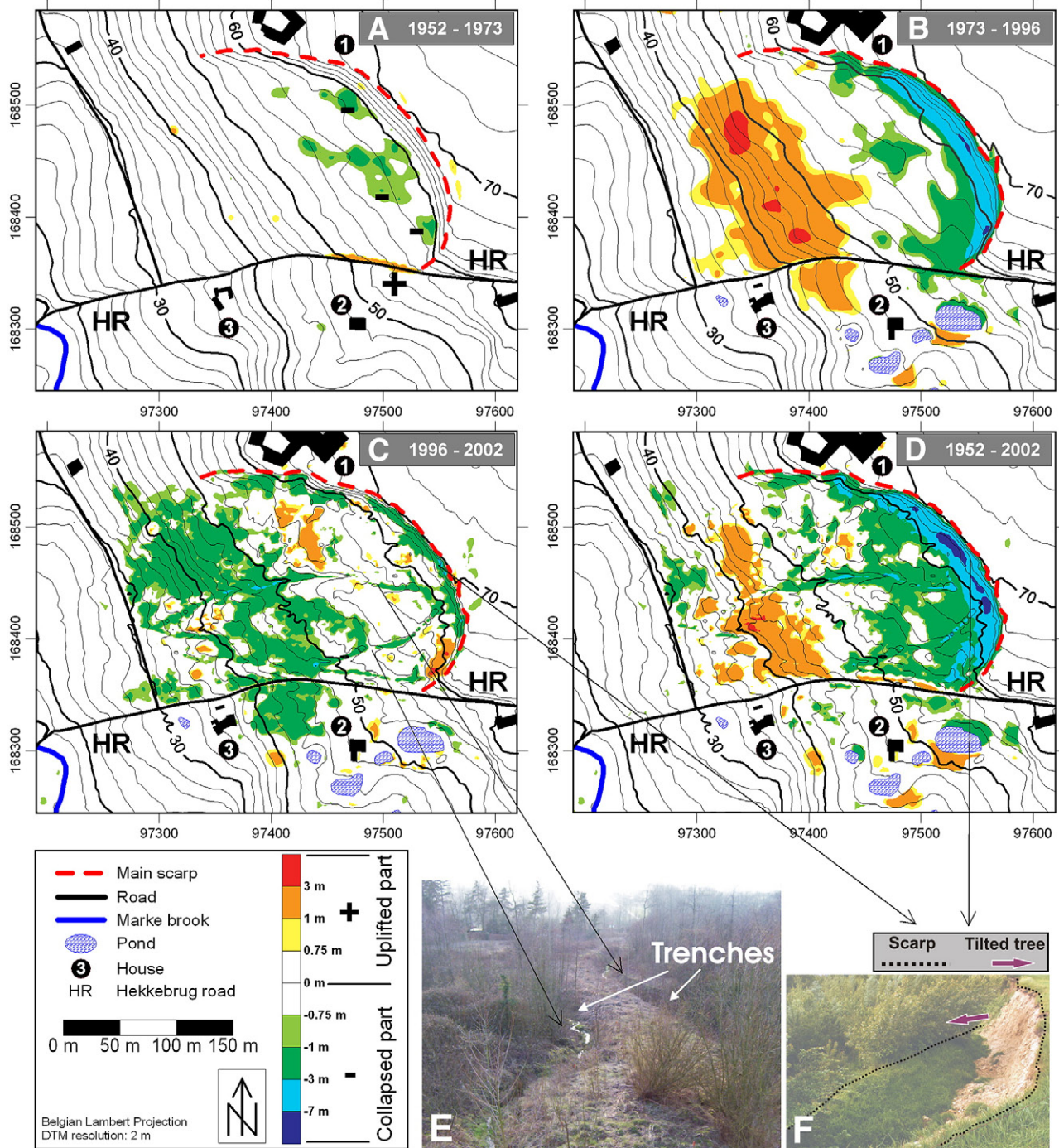
Fig. 5. Maps of vertical ground displacements within landslide 1 inferred from the comparison between the DTMs. (A): from 1952 to 1973; (B): from 1973 to 1996; (C): from 1996 to 2002; (D): from 1952 to 2002. In view (A) and (B), the underlying contour lines describe respectively the 1973 and 1996 topographies whereas the 2002 topography is shown in views (C) and (D). Only the vertical movements larger than 1σ (i.e. 0.75 m) uncertainty are represented. (E) View towards the west from the top of the main scarp of two 2-m-deep drainage trenches dug in 2000 (picture taken in February 2003). A big part of the young trees growing within the landslide are popular trees planted in place of large poplar tress cut in September 1995 after the main reactivation. (F) Main scarp reactivation occurred in March 2002 showing clearly the listric shape of the slip surface (Picture taken in May 2002).

random variables. With the assumption of normal distribution, this combined error can be used as standard deviation (Mikhail et al., 2001). Note that, since the horizontal error is a two-dimensional error, the factor for 68.3% confidence is 1.55 and 2.45 for 95% confidence (Mikhail et al., 2001). The confidence intervals associated with the ground displacements of the landslides are presented in Table 6. At a 68.3% confidence level, we are thus able to detect vertical ground displacements of ~0.70 m or larger.

We present in Fig. 5 the vertical movements identified within this recently reactivated landslide. These maps are produced with a confidence interval of 68.3%, which means that only differences in elevation larger than 1σ uncertainty are considered. For the sake of consistency, these maps are all shown with a same confidence value of ±0.75 m.

Between 1952 and 1973 (Fig. 5A), the topographical changes were very limited. The main scarp remained unchanged. The small collapses observed at the head of the slide might have resulted from de-stabilization and tension cracks in response to high groundwater levels at the contact with the Aalbeke clays as it is currently observed in other landslides of the Flemish Ardennes. The role of runoff is
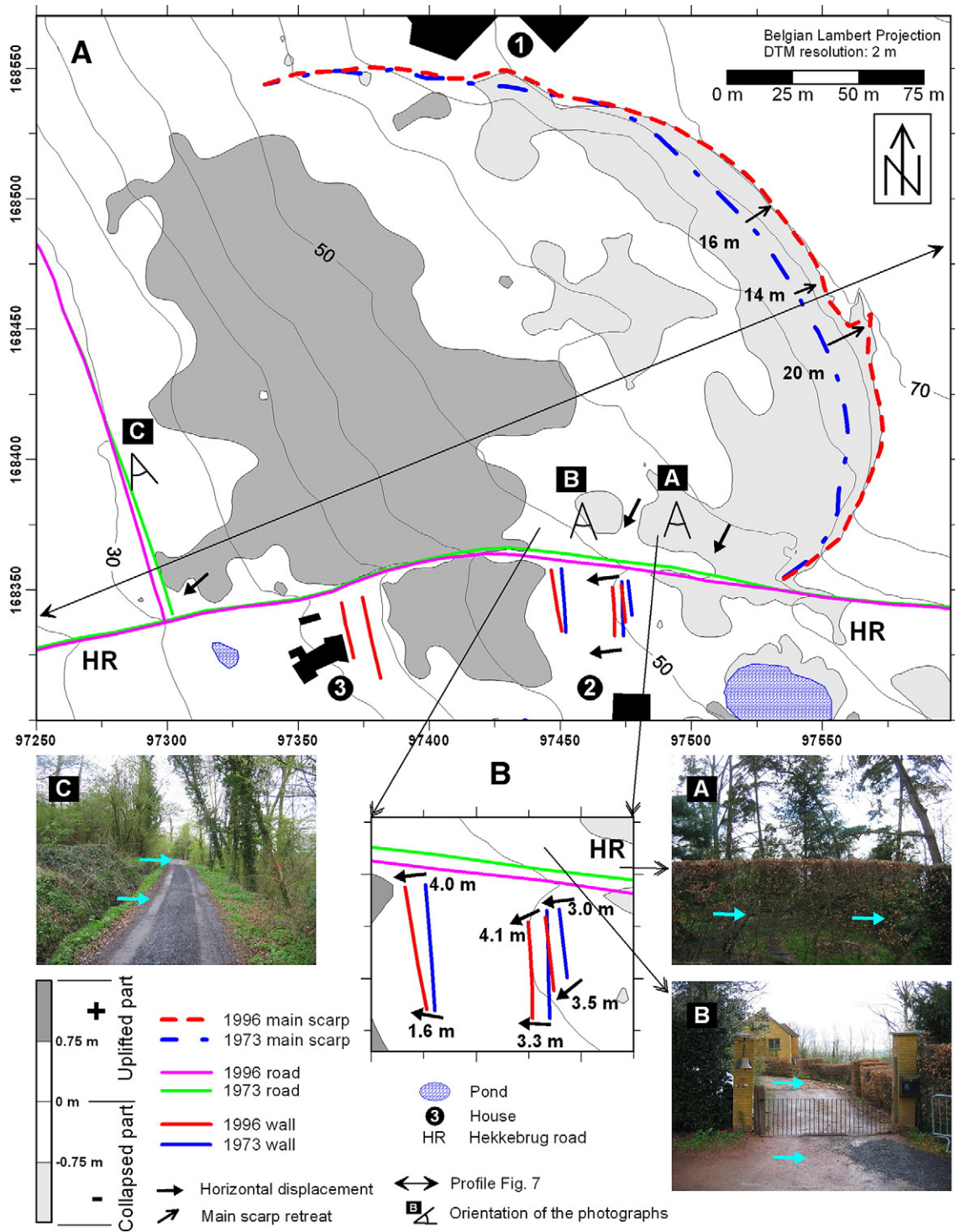
Fig. 6. Horizontal displacements measured within landslide 1 between 1973 and 1996. (A) Global view. (B) Focussed view on wall displacement close to house 2. The collapsed and uplifted parts between 1973 and 1996 are also represented. The three views, towards the south, witness to traces of horizontal displacements (April 2004). View A: picture taken from the Hekkebrug road upslope house 2. The backward toppling of the trees towards the landslide head is due to lateral displacement of the terrain. View B: picture taken from the Hekkebrug road in front of house 2. The main entry, which faced the house, has moved several meters downslope since the February 1995 reactivation. View C: picture taken on the road crossing the toe of the landslide. The backward toppling of the trees towards the landslide head is also due to lateral displacement of the terrain.

poorly known. No data and field work are available and one even ignores whether it induced a net loss of volume within the landslide, or rather brought material from upslope of the main scarp. Runoff was however probably of little importance due to the presence of a forested band upslope of the landslide head during all this period (Dewitte, 2006). The elongated zone of uplift observed along the Hekkebrug road north of house 2 was due to improvement works that

consisted in adding layers of stone bricks and asphalt to increase road accessibility (Van Den Eeckhaut et al., 2007a).

By contrast, significant movements occurred during the 1973–1996 period (Fig. 5B), revealing a typical rotational pattern, with a subsiding zone at the head, an intermediate area without vertical displacement, and an uplifted zone of accumulation towards the foot of the landslide (Dikau et al., 1996). Immediately downslope of the main scarp, large
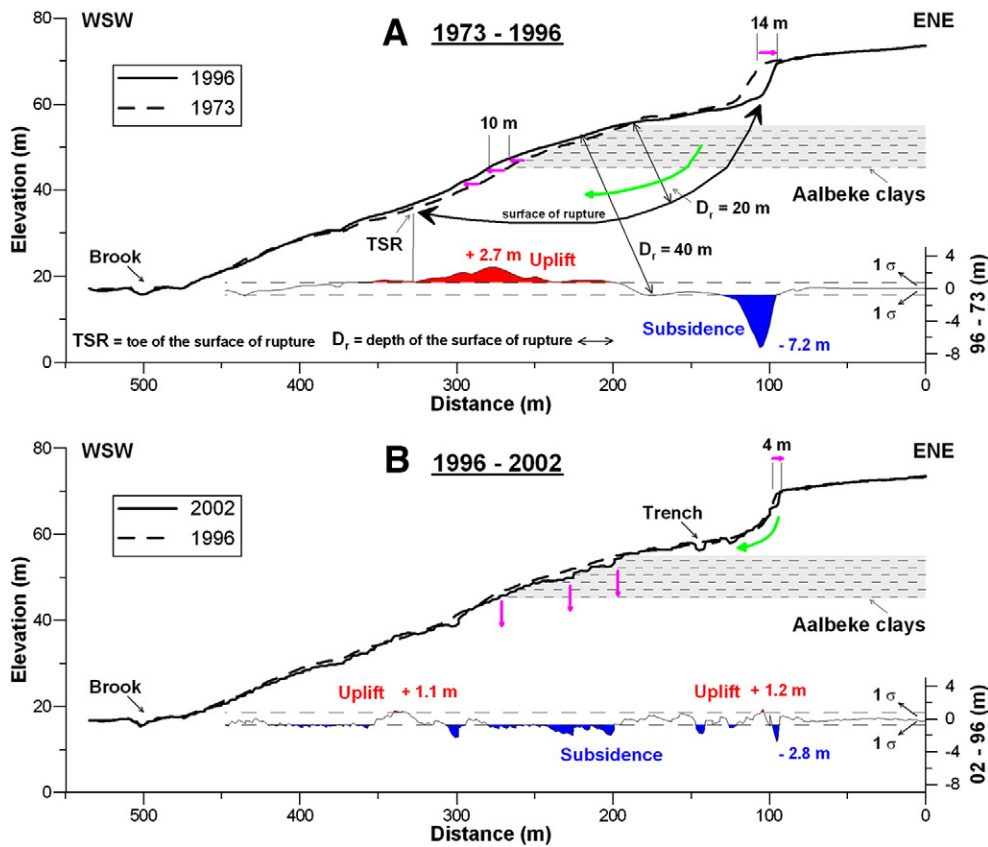
Fig. 7. DTM cross-sections of landslide 1 compared with the vertical displacements. (A) Ground displacements between 1973 and 1996. (B) Ground displacements between 1996 and 2002. Lateral motion of the main scarps and ridges are represented with horizontal arrows, vertical motions with vertical arrows, and rotational motions with curved arrows. The curve associated with the second *Y*-axis (on the right) corresponds to the vertical displacements extracted from the differential DTMs. The empty area between the two horizontal dashed lines delimits the $\pm 1\sigma$ confidence band resulting from the DTM subtraction. Only the vertical movements in excess of $\pm 1\sigma$ (i.e. 0.75 m) uncertainty are represented, which delimits the collapsed and uplifted parts. For each curve, the maximum and minimum vertical displacements are noted. The profiles are located on Fig. 6.

values of apparent collapse, corresponding to the height of the scarp (~7 m), actually indicate a scarp retreat. The amount of retreat can be approximated by the width of the band of collapsed terrain and reaches locally 15 m. The ground changes identified around the ponds near house 2 (Fig. 5B and C) are related to the construction of a garden in 1993. Note that the areas unaffected by the landslide, upslope of the main scarp, show no significant height difference between the two models, thus validating the comparison.

A study by Van Den Eeckhaut et al. (2007a) pointed out that the movements of the 1973–1996 period were mainly due to the reactivation event that occurred in February 1995. This reactivation was triggered by the heavy rainfall of the winter 1994–1995. Their effect was enhanced by increased surface runoff resulting from the development of cultivated areas that expose bare soils in winter upstream of the main scarp, with the consequence of an increase of the quantity of water directed to the landslide. Moreover, the artificial loads aimed at the improvement of the Hekkebrug road and the digging of several ponds close to house 2, and the absence of well-maintained drainage ditches after the cessation of the agricultural activities in the landslide in the 50 s contributed also to reactivation.

After 1996 (Fig. 5C), a decrease of the landslide activity was observed. It is characterized by the subsidence of large areas within the landslide, due mainly to compaction in response notably to the digging of two 2-m-deep trenches across the affected area in 2000 (Fig. 5C and E). Starting from the base of the main scarp, these trenches of ~250 m in length (total volume of both trenches=6000 m³) drain the water springing from the aquifer perched above the Aalbeke clays, and the runoff water. Subsequently, little displacement has been observed in

the zone of accumulation since 2001 (Van Den Eeckhaut et al., 2007a). The main scarp however was still active during this period as pictured in Fig. 5F. This soil slice of ~25 m length and 4 m width collapsed in March 2002. Soil material was also artificially removed and displaced within the landslide, explaining e.g., the anomalous uplift part just downslope of the main scarp close to the Hekkebrug road. Fig. 5D sums up the vertical ground displacements induced by the landslide reactivation and human intervention mainly since February 1995.

The volume change of the landslide can be estimated from the comparison of the DTMs (Weber and Herrmann, 2000; van Westen and Getahun, 2003; Baldi et al., 2005; Hapke, 2005; Brückl et al., 2006; Chen et al., 2006). According to this comparison, and removing road improvements from the computation, a loss of volume of ~5000± 1000 m³ was recorded between 1952 and 1973. Between 1973 and 1996, ~37000±5000 m³ were lost in the upper part of the landslide while ~38000±6000 m³ were added downslope. This slightly positive balance is likely to result from soil decompaction during sliding. However, the alculated volume expansion is probably underestimated because it also includes collapse and/or erosion of the slipped mass prior the reactivation (1973–1995). From 1996 to 2002, a loss of volume of ~35000±6000 m³ was detected. This loss of volume is high in comparison with the loss calculated between 1952 and 1973. Insofar as it would not result from problem of vertical inaccuracy induced by the intervention of another operator for the extraction of the LIDAR data, this difference resulted mainly from natural and artificial compaction of the recently displaced soil, and an unknown but possibly high amount of erosion induced by the improvements works linked partly to the construction of the two longitudinal drains (Fig. 5C and E).

5.2. Horizontal displacements

Several authors computed landslide horizontal displacements from multi-temporal ortho-rectified aerial photographs (e.g. Kääb, 2002; Casson et al., 2003). However, this technique was not applied here due to the scarcity of homologous points between different epochs within the landslide (Dewitte, 2006). The only way to compute horizontal displacements was then to compare the 3D positions of visually well-identifiable geomorphological features (Powers et al., 1996; Gentili et al., 2002).

We measured horizontal ground displacements both at the main scarp and within the landslide (Fig. 6). As mentioned above, the main scarp is located at the border of a plateau, and its retreat may be compared to a horizontal displacement, locally reaching 20 m between February 1995 and April 2006 (Fig. 6A). Obviously, this retreat did not result from a single reactivation affecting the whole scarp, but rather from successive collapses like that observed in 2002 (Fig. 5F).

The position of walls located between houses 2 and 3 was also measured in 1973 and 1996 (Fig. 6). Whereas the walls next to house 3 were not affected by the reactivation, the displacements of the walls in front of house 2 clearly testify to the lateral movement of this area (Fig. 6B+pictures). These movements were generally larger along the road (Fig. 6B), i.e. closer to the centre of the moving mass where the shear strength is lower (Powers et al., 1996). Road displacements within the transfer area also bear witness to lateral motion (Fig. 6), but no well-identifiable point allowed an accurate estimate of movement.

Topographic profiles are also very illustrative of the combination of vertical and horizontal displacements (Fig. 7). Fig. 7A shows that the main scarp retreat, amounting to 14 m in this profile, is clearly associated with the zone of the highest subsidence at the landslide head. According to the conceptual model developed by Casson et al. (2005) for rotational landslides, the distribution of the topographic variations between 1973 and 1996 corresponds to a large rotation angle dividing the landslide in three areas (depletion–transfer–accumulation). According to this model, the distribution of elevation changes within the profile 1973–1996, the shape of the visible part of the surface of rupture at the landslide head, and the alternation of subhorizontal clayey sand and clay layers suggest that the surface of rupture of the February 1995 reactivation is situated at a depth of ~20 m (Fig. 7A). It is in contact with the Aalbeke clays and stretches on a length of ~220 m (between 100 and 320 m from the origin of the profile). The uplift in the zone of accumulation is not a true vertical movement of the ground, but mainly the effect of the downslope lateral displacement of the slipped mass along the curved rupture surface (Fig. 7A). Due to the movement along this curved surface of rupture, the horizontal component of this displacement is therefore lower than the horizontal distance between the two profiles (10 m) that would result from a movement on a horizontal sliding plane. Likewise, the transfer area where no vertical displacement of the surface is observed between the collapsed and uplifted parts of the landslide corresponds to a zone of mainly horizontal but smaller motion. This model agrees with the values of lateral displacement measured at walls (Fig. 6B). The small uplifts located downslope of the intersection between the lower part of the surface of rupture and the original ground surface; i.e. the toe of the surface of rupture (Fig. 7A), correspond very well with several small earth flows which followed the main reactivation (Van Den Eeckhaut et al., 2007a).

An interesting issue is to know whether this deep reactivation affected the pre-existing rupture surface of the landslide or developed into the landslide debris. Electric resistivity profiles measurements carried out across a similar but dormant rotational earth slide by Van Den Eeckhaut et al. (2007b) revealed a surface of rupture at 15 m depth, i.e. pretty similar to what we found for the reactivation. In addition, their surface of rupture was also in contact with the sensitive clays of the Aalbeke Member (Fig. 7A). Dewitte and Demoulin (2005) however estimated a depth of the surface of rupture of landslide 1 of 40 m, which seems somewhat exaggerated (Fig. 7A). Actually, their measurements relied on the hypothesis that the landslide was a single rotational slide. Yet, this landslide, as many others of the Flemish Ardennes and in particular that studied by Van Den Eeckhaut et al. (2007b), is more probably a multiple rotational slide. Therefore, a part of the ancient surface of rupture of the landslide was probably re-used by the February 1995 reactivation and, consequently, both surfaces of rupture could be very similar. Supposing a depth of the surface of rupture $D_r=20$ m, and taking the length and width of the rupture surface as respectively $L_r=266$ m and $W_r=226$ m (Dewitte and Demoulin, 2005), the initial volume of material before the landslide moved, Vol_r can be computed as (Cruden and Varnes, 1996):

$$Vol_r = \frac{1}{6}\pi D_r \times W_r \times L_r. \tag{1}$$

A volume of ~625 000 m^3 is computed, i.e. half the volume computed by Dewitte and Demoulin (2005).

The 1996–2002 comparison of the topographic profiles shows a succession of positive and negative vertical variations of topography (Fig. 7B). Until 2000 and the construction of the two drainage trenches, several flow-like reactivations affected the zone of accumulation (Van Den Eeckhaut et al., 2007a). Starting from the top, the first subsidence/uplift succession is due to the reactivation of the main scarp in March 2002 (e.g. Fig. 5F). According to the model of Casson et al. (2005) this profile corresponds to a weak rotation angle. Therefore, this reactivation did not probably affect the landslide as deeply as the reactivation of February 1995, so that compaction dominated in the largest part of the zone of accumulation. Some of the topographic variations in this area were also the result of anthropogenic material displacements.

6. Conclusion

This research aimed at describing and understanding the kinematics of small landslide reactivation in the Flemish Ardennes through the use of multi-temporal DTMs. It demonstrated the effectiveness of multi-temporal DTMs, constructed from aerial stereophotogrammetry using standard photographs and airborne LIDAR data, in retrieving small ground displacements over a period of several decades, and discussing the superficial and inner landslide kinematics.

An example of ground motion analysis has been given for one representative landslide, showing the spatial and temporal variability of the displacements. The observed height changes highlight the rotational pattern associated with a reactivation in February 1995, and the later compaction as well. Estimates of the horizontal displacements corroborate the analysis.

References

Antonello, G., Casagli, N., Farina, P., Leva, D., Nico, G., Sieber, A.J., Tarchi, D., 2004. Ground-based SAR interferometry for monitoring mass movements. Landslides 1 (1), 21–28.

Baldi, P., Fabris, M., Marsella, M., Monticelli, R., 2005. Monitoring the morphological evolution of the Sciara del Fuoco during the 2002–2003 Stromboli eruption using multi-temporal photogrammetry. ISPRS Journal of Photogrammetry and Remote Sensing 59 (4), 199–211.

Berthier, E., Vadon, H., Baratoux, D., Arnaud, Y., Vincent, C., Feigl, K.L., Rémy, F., Legrésy, B., 2005. Surface motion of mountain glaciers derived from satellite optical imagery. Remote Sensing of Environment 95 (1), 14–28.

Borradaile, G., 2003. Statistics of Earth Science Data: Their Distribution in Time, Space, and Orientation. Springer-Verlag, Berlin. 351 pp.

Brückl, E., Brunner, F.K., Kraus, K., 2006. Kinematics of a deep-seated landslide derived from photogrammetric, GPS and geophysical data. Engineering Geology 88 (3–4), 149–159.

Buiten, H.J., van Putten, B., 1997. Quality assessment of remote sensing image registration — analysis and testing of control point residuals. ISPRS Journal of Photogrammetry and Remote Sensing 52 (2), 57–73.

Casson, B., Delacourt, C., Baratoux, D., Allemand, P., 2003. Seventeen years of the "La Clapiere" landslide evolution analysed from ortho-rectified aerial photographs. Engineering Geology 68 (1–2), 123–139.

Casson, B., Delacourt, C., Allemand, P., 2005. Contribution of multi-temporal remote sensing images to characterize landslide slip surface — application to the La Clapiere landslide France). Natural Hazards and Earth System Sciences 5 (3), 425–437.

Chandler, J., 1999. Effective application of automated digital photogrammetry for geomorphological research. Earth Surface Processes and Landforms 24 (1), 51–63.

Chaplot, V., Darboux, F., Bourennane, H., Leguedois, S., Silvera, N., Phachomphon, K., 2006. Accuracy of interpolation techniques for the derivation of digital elevation models in relation to landform types and data density. Geomorphology 77 (1–2), 126–141.

Chen, R.F., Chang, K.J., Angelier, J., Chan, Y.C., Deffontaines, B., Lee, C.T., Lin, M.L., 2006. Topographical changes revealed by high-resolution airborne LiDAR data: the 1999 Tsaoling landslide induced by the Chi-Chi earthquake. Engineering Geology 88 (3–4), 160–172.

Coe, J.A., Ellis, W.L., Godt, J.W., Savage, W.Z., Savage, J.E., Michael, J.A., Kibler, J.D., Powers, P.S., Lidke, D.J., Debray, S., 2003. Seasonal movement of the Slumgullion landslide determined from Global Positioning System surveys and field instrumentation, July 1998–March 2002. Engineering Geology 68 (1–2), 67–101.

Cruden, D.M., Varnes, D.J., 1996. Landslide types and processes. In: Turner, A.K., Schuster, R.L. (Eds.), Landslides: investigation and mitigation. Transportation Research Board, Special Report 247, National Research Council. National Academy Press, Washington D.C., pp. 36–75.

DEM of Flanders, 2007. Digital elevation model of Flanders (obtained by laserscanning). http://www.gisvlaanderen.be/gis/diensten/geo-vlaanderen/?catid=82007.

Demoulin, A., 2006. Monitoring and mapping landslide displacements: a combined DGPS-stereophotogrammetric approach for detailed short- and long-term rate estimates. Terra Nova 18 (4), 290–298.

Dewitte, O., 2006. Kinematics of landslides in the Oudenaarde area and prediction of their reactivation: a probabilistic approach, Ph.D. Thesis, University of Liège, Liège, 213 pp.

Dewitte, O., Demoulin, A., 2005. Morphometry and kinematics of landslides inferred from precise DTMs in West Belgium. Natural Hazards and Earth System Sciences 5 (2), 259–265.

Dewitte, O., Chung, C.-J., Demoulin, A., 2006. Reactivation hazard mapping for ancient landslides in West Belgium. Natural Hazards and Earth System Sciences 6 (4), 653–662.

Dikau, R., Brunsden, D., L.S., M.-L., Isben (Eds.), 1996. Landslide recognition. Identification, Movement and Causes. International Association of Geomrphologists, vol. 5. Wiley, Chichester. 274 pp.

Fabris, M., Pesci, A., 2005. Automated DEM extraction in digital aerial photogrammetry: precisions and validation for mass movement monitoring. Annals of Geophysics 48 (6), 973–988.

Gentili, G., Giusti, E., Pizzaferri, G., 2002. Photogrammetric techniques for the investigation of the Cornoglio landslide. In: Allison, R.J. (Ed.), Applied geomorphology: theory and practice. International Association of Geomorphologist, Publication No. 10. Wiley, Chichester, pp. 39–48.

Glenn, N.F., Streutker, D.R., Chadwick, D.J., Thackray, G.D., Dorsch, S.J., 2006. Analysis of LiDAR-derived topographic information for characterizing and differentiating landslide morphology and activity. Geomorphology 73 (1–2), 131–148.

Goovaerts, P., 1997. Geostatistics for natural resources evaluation. Applied geostatistics series. Oxford University Press, Oxford. 483 pp.

Hancock, G., Willgoose, G., 2001. The production of digital elevation models for experimental model landscapes. Earth Surface Processes and Landforms 26 (5), 475–490.

Hapke, C.J., 2005. Estimation of regional material yield from coastal landslides based on historical digital terrain modelling. Earth Surface Processes and Landforms 30 (6), 679–697.

Higgitt, D.L., Warburton, J., 1999. Applications of differential GPS in upland fluvial geomorphology. Geomorphology 29 (1–2), 121–134.

Jacobs, P., De Ceukelaire, M., De Breuck, W., De Moor, G., 1999. Toelichtingen bij de geologische kaart van België - Wlaams Gewest, Kaartblad (29) Kortrijk 1:50.000. Ministerie van Economische Zaken and Ministerie van de Vlaamse Gemeenschap, 68 pp.

Kääb, A., 2002. Monitoring high-mountain terrain deformation from repeated air- and spaceborne optical data: examples using digital aerial imagery and ASTER data. ISPRS Journal of Photogrammetry and Remote Sensing 57 (1–2), 39–52.

Kasser, M., Egels, Y., 2001. Photogrammétrie numérique. Collection ENSG - IGN. Hermes, Paris. 379 pp.

Keefer, D.K., 1984. Landslides caused by earthquakes. Geological Society of America Bulletin 95 (4), 406–421.

Kraus, K., Waldhäusl, P., 1994. Photogrammetry: Fundamentals and Standard Processes, 1. Dümmler Verlag, Bonn. 397 pp.

Lantuit, H., Pollard, W.H., 2005. Temporal stereophotogrammetric analysis of retrogressive thaw slumps on Herschel Island, Yukon territory. Natural Hazards and Earth System Sciences 5 (3), 413–423.

LH Systems, 1999. Digital Photogrammetric Workstation: SOCET SET Version 4.2 User's Manual. Marconi Integrated Systems Inc. 802 pp.

Malet, J.P., Maquaire, O., Calais, E., 2002. The use of Global Positioning System techniques for the continuous monitoring of landslides: application to the Super-Sauze earthflow (Alpes-de-Haute-Provence, France). Geomorphology 43 (1–2), 33–54.

Mantovani, F., Soeters, R., VanWesten, C.J., 1996. Remote sensing techniques for landslide studies and hazard zonation in Europe. Geomorphology 15 (3–4), 213–225.

McKean, J., Roering, J., 2004. Objective landslide detection and surface morphology mapping using high-resolution airborne laser altimetry. Geomorphology 57 (3–4), 331–351.

Metternicht, G., Hurni, L., Gogu, R., 2005. Remote sensing of landslides: an analysis of the potential contribution to geo-spatial systems for hazard assessment in mountainous environments. Remote Sensing of Environment 98 (2–3), 284–303.

Mikhail, E.M., Bethel, J.S., McGlone, J.C., 2001. Introduction to modern photogrammetry. Wiley, New York. 479 pp.

Nico, G., Rutigliano, P., Benedetto, C., Vespe, R., 2005. Terrain modelling by kinematical GPS survey. Natural Hazards and Earth System Sciences 5 (2), 293–299.

Oka, N., 1998. Application of photogrammetry to the field observation of failed slopes. Engineering Geology 50 (1–2), 85–100.

Powers, P.S., Chiarle, M., Savage, W.Z., 1996. A digital photogrammetric method for measuring horizontal surficial movements on the Slumgullion earthflow, Hinsdale county, Colorado. Computers & Geosciences 22 (6), 651–663.

Siska, P.P., Goovaerts, P., Hung, I.K., Bryant, V.M., 2005. Predicting ordinary kriging errors caused by surface roughness and dissectivity. Earth Surface Processes and Landforms 30 (5), 601–612.

Squarzoni, C., Delacourt, C., Allemand, P., 2005. Differential single-frequency GPS monitoring of the La Valette landslide (French Alps). Engineering Geology 79 (3–4), 215–229.

Tarchi, D., Casagli, N., Fanti, R., Leva, D.D., Luzi, G., Pasuto, A., Pieraccini, M., Silvano, S., 2003. Landslide monitoring by using ground-based SAR interferometry: an example of application to the Tessina landslide in Italy. Engineering Geology 68 (1–2), 15–30.

Van Den Eeckhaut, M., 2006. Spatial and temporal patterns of landslide in hilly regions. The Flemish Ardennes (Belgium). Katholieke Universiteit Leuven, Leuven. 250 pp.

Van Den Eeckhaut, M., Poesen, J., Verstraeten, G., Vanacker, V., Moeyersons, J., Nyssen, J., van Beek, L.P.H., 2005. The effectiveness of hillshade maps and expert knowledge in mapping old deep-seated landslides. Geomorphology 67 (3–4), 351–363.

Van Den Eeckhaut, M., Poesen, J., Dewitte, O., Demoulin, A., De Bo, H., Vanmaercke-Gottigny, M.C., 2007a. Reactivation of old landslides: lessons learned from a case-study in the Flemish Ardennes (Belgium). Soil Use and Management 23 (2), 200–211.

Van Den Eeckhaut, M., Verstraeten, G., Poesen, J., 2007b. Morphology and internal structure of a dormant landslide in a hilly area: the Collinabos landslide (Belgium). Geomorphology 89 (3–4), 258–273.

van Westen, C.J., Getahun, F.L., 2003. Analyzing the evolution of the Tessina landslide using aerial photographs and digital elevation models. Geomorphology 54 (1–2), 77–89.

Weber, D., Herrmann, A., 2000. Contribution de la photogrammétrie numérique à l'étude spatio-temporelle de versants instables: l'exemple du glissement de Super-Sauze (Alpes-de-Haute-Provence). Bulletin de la Société géologique de France 171 (6), 637–648.